A multiscale nested modeling framework to simulate the interaction of surface gravity waves with nonlinear internal gravity waves

Oliver B. Fringer
Department of Civil and Environmental Engineering, Stanford University, Stanford, CA, 94305
phone: (650) 725-6878 fax: (650) 725-9720 email:fringer@stanford.edu

Award number: N00014-15-1-2287

LONG-TERM GOALS

Our long-term goal is to develop a multiscale nested modeling framework that simulates, with the finest resolution being centimeter scale, surface mixed layer processes arising from the combined action of tides, winds and mesoscale currents. Issues related to nesting of models designed to study phenomena at different scales will be studied, including how to nest the regional and nonhydrostatic SUNTANS model within the global HYCOM model, as well as nesting of small-scale LES codes into the SUNTANS model.

OBJECTIVES

As a model problem of mixed-layer dynamics involving numerous physical processes acting over a wide range of spatio-temporal scales, we will focus on the interaction of surface and internal gravity waves in the South China Sea. Our objective is to study surface gravity wave evolution and spectra in the presence of surface currents arising from strongly nonlinear internal gravity waves. We will focus on understanding the impact of tidal, seasonal, and mesoscale variability of the internal wave field and how it impacts the surface waves.

APPROACH

We are working on this project in collaboration with Lian Shen from the University of Minnesota and Dong Ko from the Naval Research Laboratory, Stennis Space Center. The focus is on the problem of modification of the wind-wave field by internal wave surface currents, a process that can be validated with both in-situ observations and synthetic aperature radar (SAR) imagery which shows distinct internal solitary wave (ISW) signatures throughout the South China Sea (Jackson et al. 2013). Despite advances in internal wave modeling of the South China Sea (Simmons et al. 2011) and SAR imaging techniques of ISWs (Xue et al. 2013), there is no predictive ability of ISW dynamics in the South China Sea owing to the computational expense associated with computing nonhydrostatic effects inherent to ISWs. Furthermore, extensive theory exists to explain the sea-surface expression of ISWs, but it is based on idealized internal wave theory and no three-dimensional models have been applied to understand or predict the surface wave field and how it interacts with the internal wave-driven surface currents. To this end, we are performing simulations with a series of nested models to understand the three-dimensional dynamics governing the interaction of surface and internal gravity waves. Specific question we are addressing include:

1) How well do weakly nonlinear ISW theories predict the evolution of ISWs in the presence of a variable mesoscale background field?
2) How does the wind-wave field evolve in the presence of surface currents driven by ISWs?
3) How does the surface gravity wave field above ISWs modify the mixing and dissipation in the mixed layer?
4) What specific parameters related to ISWs enhance or limit their impact on the surface gravity wave spectrum? How does this affect the detectability of ISWs in SAR imagery?
5) How does the seasonal variability of ISW currents impact the surface gravity wave spectra?

To simulate finescale processes related to surface gravity waves, a large-eddy simulation (LES) code that simulates turbulence-wave interactions on a wave-surface-fitted grid and a nonlinear wave-field simulation code is being employed (Yang et al. 2013, 2014). The LES code will be driven by currents from a high-resolution, nonhydrostatic, hybrid-coordinate model based on SUNTANS (Fringer et al. 2006) that will simulate ISW evolution in the SCS. Although the SUNTANS model was applied to simulate ISWs in the SCS (Zhang et al. 2011), that implementation did not incorporate sufficient resolution to resolve the ISWs. In this proposal we will resolve the leading-order ISW dynamics by performing SUNTANS simulations in a limited region of the SCS using the nonhydrostatic isopycnal-coordinate method of Vitousek and Fringer (2014). Initial and boundary conditions for the hybrid-coordinate SUNTANS model will be obtained from the East Asian Seas Nowcast/Forecast System (EASNFS), which computes the generation of internal tides and includes assimilated seasonal and mesoscale variability (Ko et al. 2014). The low-frequency variability from EASNFS will be assimilated into the SUNTANS model using a novel scale-separation technique that assimilates low-frequency data without compromising high-frequency variability related to internal waves. Ultimately, because EASNFS is also nested within Global NCOM (Rhodes et al. 2002), the proposed work will simulate surface-internal wave interactions through nesting of four models over spatial scales ranging from 1000 km down to 10 cm. Below we provide details of the individual modeling components.

WORK COMPLETED

We have developed a cut-cell approach for the SUNTANS model that enables the z-level structure of the hybrid-grid to accurately resolve bottom bathymetry.

RESULTS

In the process of developing the hybrid-grid implementation for the SUNTANS model, we found it necessary to retain the bottom-following nature of sigma or isopycnal coordinates when reverting to a z-level grid. This ensures that the bathymetry is similarly represented using all grid types and is important for mass- and momentum conservation when transitioning between the grid types in the hybrid grid approach. The bathymetry can be “followed” with z-level grids using cut cells whereby, using typical approaches in Navier-Stokes solvers (e.g. Tucker and Pan 2000) or ocean models (Adcroft et al. 1997; MITgcm), the finite-volume equations on the Cartesian grid cells are modified to account for bathymetry in the bottom-most cells. In contrast to the stair- or partial-stepping approach, in which it is assumed that the bottom of the bottom-most cells are flat, the cut-cell approach ensures that the vertices of the cells near the bed match the bottom bathymetry, as shown in Figure 1. Although the functional form of the bathymetry can be assigned arbitrarily, the typical approach is to assume that it is piecewise linear in each

cell. Our approach most closely follows that in the MITgcm ocean model (Adcroft et al. 1997), although we adapt the method for the unstructured grid in SUNTANS.

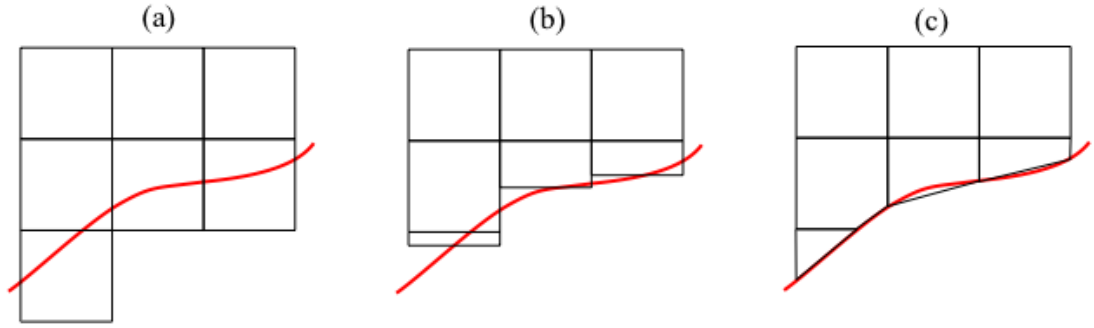

Figure 1: Representation of the bottom bathymetry (red) on a Cartesian or z-level grid using stair-stepping (a), partial stepping (b), or piecewise-linear cut cells (c).

Implementation of the cut-cell approach on an unstructured grid requires modification of the terms in the finite-volume equations to account for changes in cell volumes and face areas that arise when the cell is cut by the piecewise linear bottom. A simple example can be seen in Figure 2, in which an unstructured, prismatic cell is cut by a piecewise-linear bottom. The finite-volume form of the divergence of an arbitrary flux $\vec{F}$ in the bottom-most cell on the stair-stepped grid in Figure 2(a) is given by (after assuming there is no flux through the bottom face)

$$\nabla \cdot \vec{F} \approx \frac{1}{V}\left(\sum F_{n,v} A_{f,v} + F_{n,t} A_t\right) = \frac{1}{V}\left(\sum F_{n,v} l_{f,v} \Delta z + F_{n,t} A_t\right), \tag{1}$$

where $F_{n,v}$ and $F_{n,t}$ are the normal components of the flux at the vertical and top faces, respectively, $A_{f,v}$ and A_t are the cross-sectional areas of the vertical and top faces, respectively, and $l_{f,v}$ and Δz are the length and height of the vertical faces, respectively. Equation (1) represents the advection operator in SUNTANS when $\vec{F} = \vec{u}\phi$, where ϕ is one of salinity, temperature, or one of the three Cartesian velocity components. Equation (1) also represents the left-hand side of the pressure-Poisson equation for the nonhydrostatic pressure q if $\vec{F} = \nabla q$. Finally, Equation (1) represents the diffusion operator for a scalar quantity ϕ in SUNTANS when $\vec{F} = -\gamma \nabla \phi$, where γ is the turbulent eddy-viscosity or eddy-diffusivity.

Equation (1) represents the divergence of the flux in the presence of a flat bottom. In the presence of a sloping bottom, the points at which the bed intersects the vertices of the triangular cell move from those indicated by A-B-C in Figure 2(a) to A'-B'-C' in Figure 2(b). To account for the new sloping bed, the governing discretization is similar to (1), except the cross-sectional areas and volume are modified. For example, the area of the top face, A_t, indicated by the polygon with vertices D-E-F in Figure 2(a) is modified to represent the area of the cut face indicate by the polygon with vertices D-P_2-P_1-F in Figure 2(b). To account for the altered areas of the vertical faces, the discretization employs effective heights such that the modified vertical face areas are given by $A'_{f,v} = l_{f,v} \Delta z'$. As an example, if the vertical face in Figure 2(a) indicated by the polygon with vertices A-B-D-E has area $A_{f,v}$, then the modified height of that face in the presence of the bottom slope would be given by $\Delta z' = A'_{f,v} / l_{f,v}$, where A¢$_{f,v}$ is the area of the polygon with vertices A'-P_2-D in in Figure 2(b). In this way, the original

SUNTANS model retains its structure because the heights of the vertical faces are defined regardless of whether or not there are cut cells.

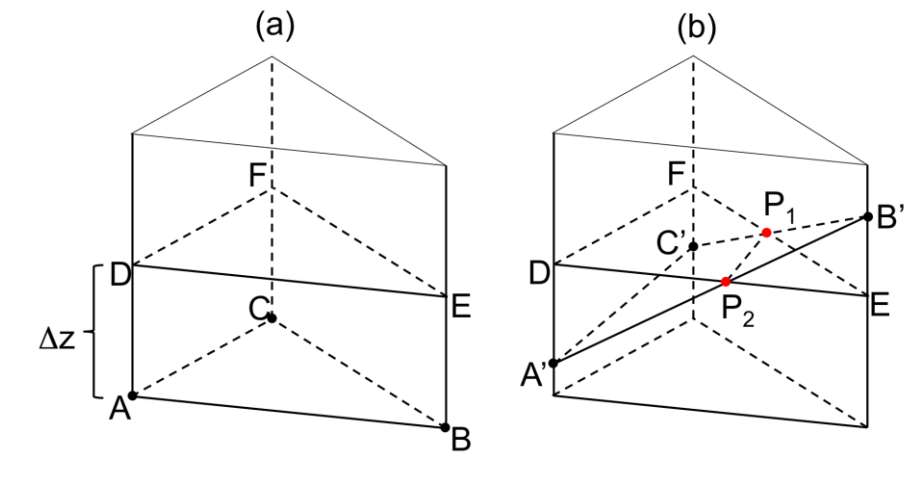

Figure 2: Depiction of a prismatic, unstructured-grid z-level arrangement using stair-stepping (a) and the cut-cell approach (b). The bathymetry in (a) is defined by the flat bottom defined by plane A-B-C, while that in (b) is defined by the plane with vertices A'-B'-C'. This plane intersects the top face of the bottom-most cell along the line segment P_1-P_2.

Modification of the cell volumes and faces in the presence of cut cells accounts for the effects of a sloping bottom on the terms in SUNTANS that are computed as the divergence of a flux with Equation (1). However, the Coriolis term in SUNTANS is not computed as the divergence of a flux and so it cannot be represented by Equation (1). Instead, the Coriolis term in SUNTANS accounts for the cut-cell geometry when reconstructing the cell-centered velocity vectors in a manner similar to Kleptsova et al. (2009), who modified the Perot (2000) scheme to account for the depths of the cell faces. The reconstructed cell-centered velocity components with cut cells are also used to compute advection of horizontal momentum in SUNTANS.

We demonstrate the effectiveness of the cut-cell method with two test cases. The first is a gravity current propagating down a slope, which is similar to a test case in Ezer and Mellor (2004). As shown in Figure 3, the test case involves a dense inflow at the left boundary of a sloping domain with a slope of 0.5 degrees. The inflow current speed is 0.88 m s^{-1} and its density anomoly is +0.7 kg m^{-3} relative to the constant background density field in the domain. The stair-stepped result in the left column of Figure 3 produces grid-scale oscillations in the vertical velocity which produces strong spurious vertical mixing and dissipation that acts to significantly decelerate the gravity current relative to the cut-cell case in the right column of Figure 3. The result is a gravity current that propagates 15% more slowly when using cut cells (3.9 m s^{-1} vs 4.6 m s^{-1}).

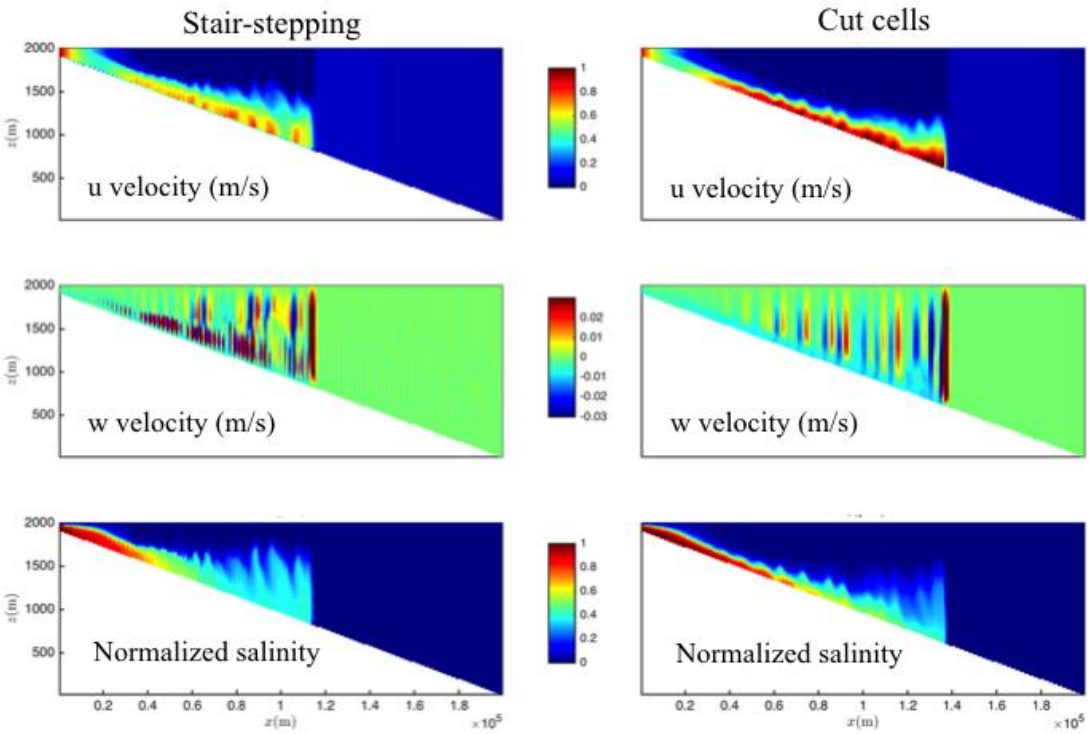

Figure 3: Velocity field and normalized salinity after 3.25 days for the gravity current test case using stair-stepping (left column) and cut cells (right column), showing how the cut-cell approach eliminates the grid-scale variations in the vertical velocity, thus reducing spurious mixing and producing a more realistic and faster gravity current.

The gravity current test case demonstrates how the cut cells enforce along-slope flows for a largely hydrostatic case. To demonstrate the effectiveness of the cut-cell method with a nonhydrostatic flow, we study the ability of the SUNTANS model to reproduce the irrotational flow field over a Gaussian bump, as shown in Figure 4. To achieve this flow field, constant inflows are specified at the left and right boundaries (the magnitude is irrelevant because all results are expressed nondimensionally), the top and bottom boundaries are assumed to be free slip, and the top boundary is assumed to be a rigid lid. With these conditions, the SUNTANS model produces the irrotational flow field shown in Figure 4 after one time-step of the nonhydrostatic pressure solver. In this case the nonhydrostatic pressure q is a surrogate for the velocity potential since it satisfies $\vec{u} = -\nabla q$. Upon enforcing a divergence-free constraint due to flow incompressibility (i.e. $\nabla \cdot \vec{u} = 0$), the result is a pressure field that satisfies the Laplace equation $\nabla^2 q = 0$. Use of cut cells produces a velocity field that is parallel to the bed (top panel of Figure 4), while stair steps lead to a discontinuous velocity field that is not parallel to the bed (bottom panel of Figure 4). The cut cell approach ensures an along-slope flow because it guarantees that the component of the pressure gradient normal to the bed is zero. That is, it ensures that $\vec{n} \cdot \vec{u} = -\vec{n} \cdot \nabla q = \partial q / \partial n = 0$. As shown in Figure 5, this implies that the cut cell method produces nonhydrostatic pressure contours that are normal to the bed, as they should be.

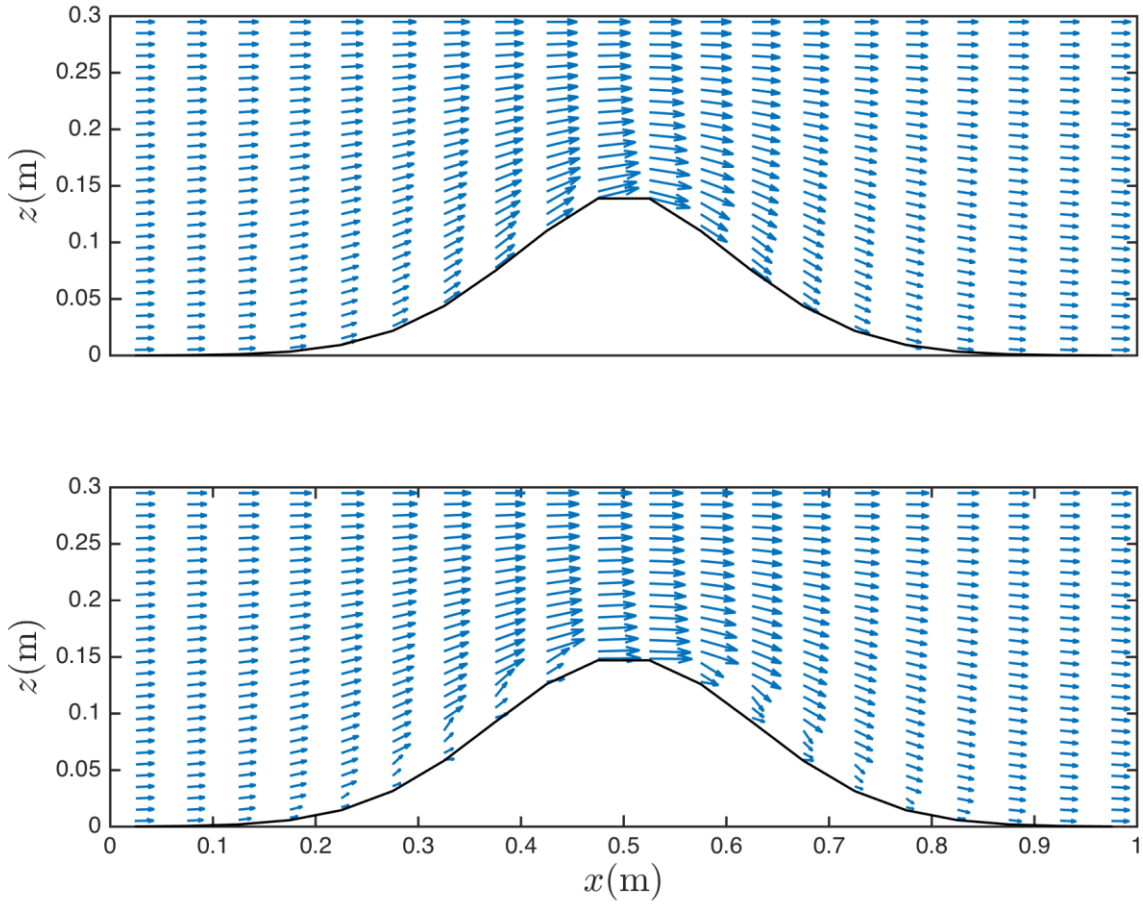

Figure 4: Velocity vectors for the irrotational flow test case over a Gaussian bump with (top panel) and without (bottom panel) the cut-cell method.

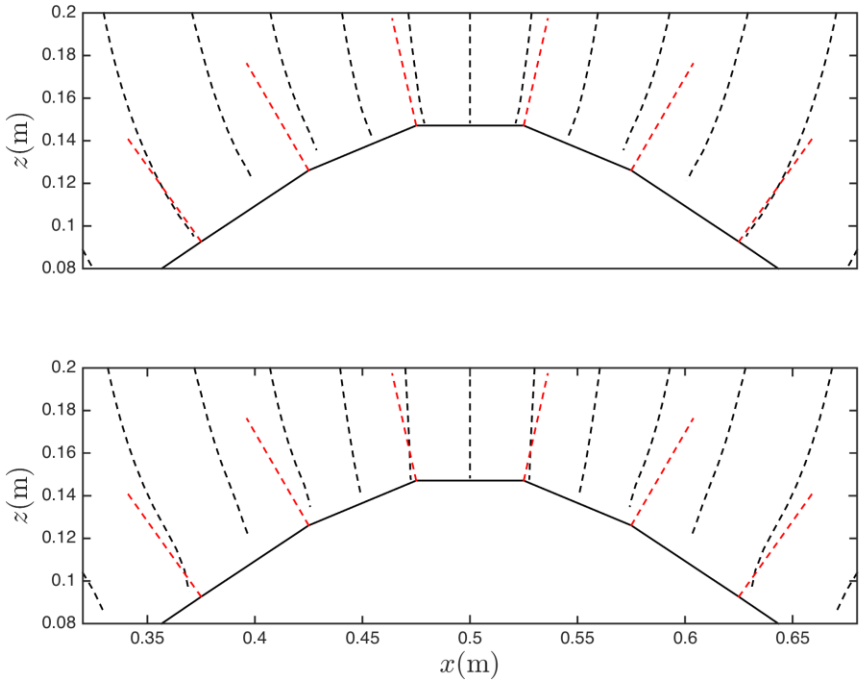

Figure 5: Nonhydrostatic pressure contours (black dashed lines) for the irrotational flow test case with (top panel) and without (bottom panel) the cut-cell method. The red dashed lines indicate the normal direction to the slope and show how they are parallel to the pressure contours when cut cells are used.

IMPACT/APPLICATIONS

High-resolution simulations using nested, nonhydrostatic modeling frameworks such as the proposed HYCOM-SUNTANS-LES nested model are crucial for understanding multiscale processes that are unresolved, and hence parameterized, in larger-scale ocean models.

RELATED PROJECTS

The HYCOM-nested SUNTANS isopycnal model is also being developed as part of the FLEAT DRI to study the interaction of the North Equatorial Current with steep topography around the island of Palau.

REFERENCES

Adcroft, A., Hill, C., Marshall, J. (1997), Representation of topography by shaved cells in a height coordinate ocean model. Monthly Weather Review, 125 (9), 2293–2315.

Ezer, T., and G. L. Mellor (2004), A generalized coordinate ocean model and a comparison of the bottom boundary layer dynamics in terrain-following and in z-level grids, Ocean Modelling, 6, 379-403.

Fringer, O.B., Gerritsen, M., and R.L. Street (2006), An unstructured-grid, finite-volume, nonhydrostatic, parallel coastal ocean simulator. Ocean Modelling, 14, 139–278.

Kleptsova, O., Pietrzak, J., and G.S. Stelling (2009), On the accurate and stable reconstruction of tangential velocities in C-grid ocean models. Ocean Modelling, 28, 118–126.

Ko, D. S., Chao, S.-Y., Wu, C.-C., and I.-I. Lin (2014), Impacts of Typhoon Megi (2010) on the South China Sea, J. Geophys. Res. Oceans, 119, 4474-4489.

Perot J. B. (2000), Conservation properties of unstructured staggered mesh schemes, J. Comput. Phys., 159, 58-89.

Rhodes, R.C., Hurlburt, H.E., Wallcraft, A.J., Barron, C.N., Martin, P.J., Smedstad, O.M., Cross, S., Metzger, E.J., Shriver, J., Kara, A., and D.S. Ko (2002), Navy real-time global modeling system, Oceanography, 15, 29–43.

Simmons, H., M.-H. Chang, Y.-T. Chang, S.-Y. Chao, O. Fringer, C.R. Jackson, and D.S. Ko (2011), Modeling and prediction of internal waves in the South China Sea, Oceanography 24(4), 88-99.

Tucker, P.G., and Z. Pan (2000) A Cartesian cut cell method for incompressible viscous flow, Applied Mathematical Modeling, 24 (8-9), 591-606.

Vitousek, S., and O. B. Fringer (2014), A nonhydrostatic, isopycnal-coordinate ocean model for internal waves, Ocean Modelling, 83, 118-144.

Xue, J., Graber, H.C., Lund, B., and R. Romeiser (2013), Amplitudes estimation of large internal solitary waves in the mid-Atlantic bight using synthetic aperture radar and marine X-band radar images. IEEE Trans. Geosci. Remote Sens., 51 (6), 3250–3258.

Yang, D., Meneveau, C., and L. Shen (2013), Dynamic modeling of sea-surface roughness for large-eddy simulation of wind over ocean wavefield, Journal of Fluid Mechanics, 726, 62–99.

Yang, D., Meneveau, C., and L. Shen (2014), Large-eddy simulation of offshore wind farm, Physics of Fluids, 26, 025101.

Zhang, Z., Fringer, O.B., and S.R. Ramp (2011), Three-dimensional, nonhydrostatic numerical simulation of nonlinear internal wave generation and propagation in the South China Sea, J. Geophys. Res., 116, C05022.